JOURNAL OF MATERIALS SCIENCE 29 (1994) 4984–4992

Interpretation of the impedance spectroscopy of cement paste via computer modelling

Part II *Dielectric response*

R. T. COVERDALE*, B. J. CHRISTENSEN*, T. O. MASON*, H. M. JENNINGS*,‡
Departments of Materials Science and Engineering and Civil Engineering‡, Northwestern University, Evanston, IL 60208, USA*

E. J. GARBOCZI
National Institute of Standards and Technology, Building Materials Division, Building 226, Room 348 B, Gaithersburg, MD 20899, USA

Dielectric properties of cement pastes are measured using impedance spectroscopy, and the effective dielectric constants of the low frequency bulk arcs are reported. The unusually high values thereby obtained, and their dependence on reaction time and water:cement ratio, are explained by the presence of microstructural features that serve to amplify the dielectric constants of the individual material phases. The dielectric properties of three-dimensional cement paste models and of simple two-dimensional models of the hypothesized microstructural features are analysed. The model results provide insight into the proposed dielectric amplification mechanism in real cement paste.

1. Introduction

Several papers have been published recently relating the impedance response of cement paste to certain aspects of the microstructure [1–9]. These reports have focused on the observed offset resistance, bulk resistance and the origin of the dielectric response of cement paste. However, the effective dielectric constant associated with the bulk arc has not been reported. Part I of this paper [10], studied the bulk resistance and the apparent "offset resistance" found in Nyquist plots of the impedance response of cement paste, using computer modelling. In Part II of this paper, computer modelling is used to help understand the dielectric response of cement paste, and in particular the *low frequency effective dielectric constant.*

Using impedance spectroscopy techniques [10, 11], the low frequency effective dielectric constant, k_{eff}, associated with the bulk arc of the Nyquist impedance plot, has been measured. k_{eff} has been found to be a function of the water:cement ratio (w/c = weight ratio of water to cement in the original mixture), and the age or degree of reaction of the paste. The quantity k_{eff} is defined in the following way [11]. A Nyquist plot that is perfectly circular in the complex impedance plane, with its centre on the real axis, can be fit to a circuit containing a perfect resistor, R, and a perfect capacitor, C, connected in parallel. The value of R is the d.c. resistance of the material, and the value of C, normalized for the geometry, gives the dielectric constant $\varepsilon = k\varepsilon_0$.

It has been found [1, 10] that the Nyquist plots for cement paste can be successfully fit by "constant phase elements", or CPEs [10, 11], which are circular arcs but with their centre depressed below the real axis. In these circuit elements, a parameter, Q, takes the place of C in the parallel r.c. circuit. If the arcs are not depressed below the axis very much, as is usually the case for cement paste, then an effective dielectric constant $k_{eff} = Q'/E_0$, where Q' is just Q but normalized for sample geometry, can be defined [11]. The parameter Q reduces to the regular capacitance, C, when the centre of the arc is on the real axis. This is the quantity reported and discussed in this paper. In the area of composites, quantities reflecting the response of an entire sample are also often denoted as "effective" or "average" quantities [12]. This same meaning also applies to the effective dielectric constant measured, as cement paste is a composite material, and the dielectric response of the entire composite is measured.

2. Experimental results

Fig. 1 shows a plot of k_{eff} versus time for a 0.4 w/c cement paste. The dashed line represents data obtained from impedance arcs that were very difficult to fit since they were barely measurable. The dashed line data are also probably not reliable because they were obtained at high frequencies (> 3 MHz) at which induction effects occur due to the experimental apparatus. The solid line is computed from data obtained from larger bulk arcs occurring at lower, more reliable frequencies. The effective dielectric constant is seen to decrease from a very large value near 90 000 and eventually levels off at a value near 4000.

0022–2461

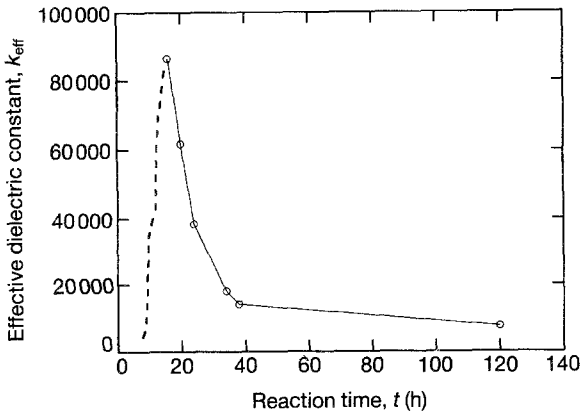

Figure 1 Experimental results for change in the effective dielectric constant, k_{eff}, as a function of reaction time for a 0.4 water:cement ratio cement paste.

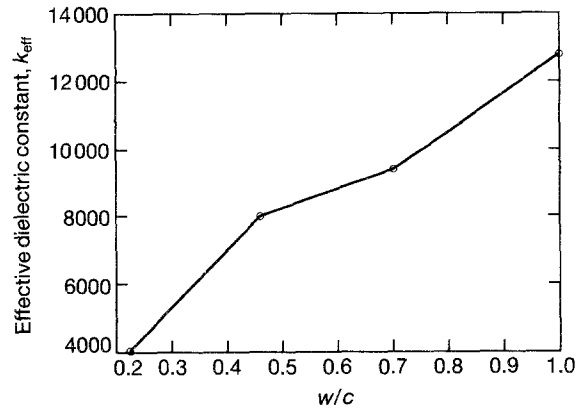

Figure 2 Experimental results for the effective dielectric constant, k_{eff}, of cement pastes hydrated for 11 months versus the water: cement ratio.

Fig. 2 shows a plot of k_{eff} versus water:cement ratio for a single Portland cement after long reaction times (11 months). It can be seen that the effective dielectric constant increases with water:cement ratio, and also that the values are still large, ranging from 4000 to above 12000 for the highest w/c pastes.

These high values are difficult to explain, especially since the material phase in the microstructure that has the highest dielectric constant would have thought to have been pore fluid, with a dielectric constant near 80 [13]. However, separate dielectric measurements of synthetic calcium silicate hydrate (C–S–H) and of pastes containing mostly C–S–H, indicate that C–S–H has an effective dielectric constant significantly higher than pore fluid, perhaps on the order of $\varepsilon_{C-S-H} = 1000$ [14]. This does not, however, explain the observed phenomena, for two reasons.

First, this value of ε_{C-S-H} is not high enough to explain the effective dielectric constant of 90000 for pastes at very early reaction times, when only a small percentage of C–S–H is present. And second, if C–S–H were responsible for the high dielectric constant of the paste, the value for the paste should increase, not decrease, with reaction time, since more C–S–H is being produced, replacing the much lower dielectric constant water and cement.

The dielectric response of cement paste has been attributed [9, 15], to electrical double layers that form at the interfaces between pore fluid and product and/or reactant surfaces. Calculations by Xie *et al.* [9] indicate that a double layer (Stern layer) in the cement system should have a dielectric constant of 17.4, which is significantly less than observed values of bulk cement paste. However, double layers are certainly present on cement particles after mixing with water, yet the bulk arc does not appear until after a significant amount of reaction product has formed ($\sim$ 12 h). Possibly, as the hydration reaction proceeds, the surfaces available to form double layers increase dramatically, which could explain the delayed appearance of the bulk arc. But this does not explain why the dielectric constant of bulk paste decreases as hydration proceeds, a process that is producing more and more free surface.

An alternative explanation of the dielectric response of cement paste is that the arrangement of phases within the microstructure provides an *amplification mechanism* that gives rise to the high values of k_{eff} observed. The "amplification mechanism" is defined as a geometrical arrangement of material phases that results in an effective dielectric constant that is much higher than the value for any individual material phase. As an example, it is noted that this phenomenon is observed in composite materials composed of an insulating and a conducting phase, where the conducting phase is very close to, but just below, its percolation threshold [16–18]. The complex geometry that gives rise to this amplification mechanism is "the existence of many almost pure conducting channels which stretch across the entire length of the system and are blocked off only by very thin barriers. Every channel of this type contributes an abnormally large capacitance, and all of these are connected in parallel" [17].

A simpler geometry that also gives rise to dielectric amplification by forcing current across thin layers of insulating material is shown in Fig. 3. This figure shows a two-dimensional schematic of a three-dimensional perfect parallel plate capacitor into which a conductive plate has been placed. The overall capacitance is affected by the thickness of the inserted plate as follows

$$C = k_{eff}\varepsilon_0 A/D = k_S\varepsilon_0 A/(D-b) = k_S\varepsilon_0 A/d = k_S\varepsilon_0(A/D)(D/d) \quad (1)$$

from which it follows that

$$k_{eff} = k_S D/d \quad (2)$$

Here k_{eff} is the true composite effective dielectric constant; k_S is the dielectric constant of the material that is in the space d; ε_0 is the permittivity of free space; A is the area of the electrodes; and D, d and b are as shown in the Fig. 3. It is clear that as b becomes larger, d becomes smaller, and the capacitance increases. This phenomenon is observed in grain boundary ceramics in which conductive grains are isolated by insulating grain boundaries [11]. The composite dielectric constant is proportional to D/d, where D is the grain size

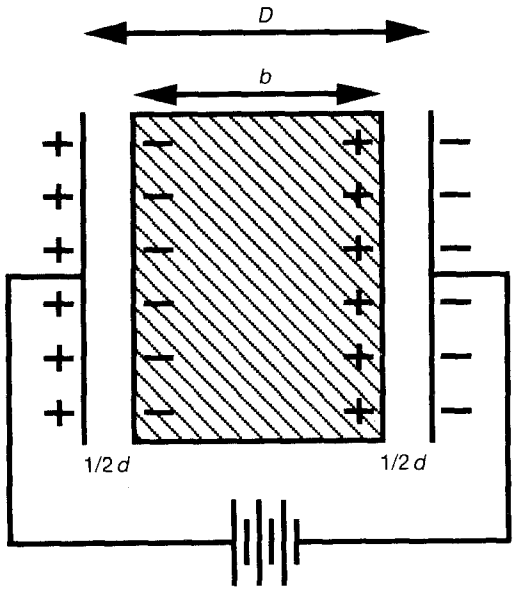

Figure 3 Schematic diagram of a parallel plate capacitor (after Feynman *et al.* [19]) with a crossbar thickness, t, of 1 pixel.

and d is the grain boundary thickness. The larger the grain size (conductor) and the thinner the grain boundary (insulator), the greater the amplification. In these materials, the high conductivity material phase is disconnected.

A similar mechanism may be responsible for the observed dielectric response in cement pastes. As the microstructure develops, relatively large (~ 20 μm) capillary pores, filled with highly conductive pore fluid, are reduced in size as reaction products fill space. Following the model shown in Fig. 3, the conductive pores would correspond to the conductive plate sandwiched between the much more insulating layers of reaction product. As hydration proceeds, capillary pore size, D, tends to decrease, and the reaction product thickness, d, tends to increase. Thus, the overall capacitance, starting out high, would then be systematically reduced as the hydration reaction proceeded. However, the isolation, or disconnection, of the conductive pore phase, as pictured in Fig. 3 and found in grain boundary ceramics [11], is not necessary to produce the observed phenomena. Computer simulation modelling is next used to explore the possibility that highly tortuous pathways of *continuous* conductive pore fluid channel the current into regions where it is forced to drop across thin layers of insulating material, thus producing a high value of k_{eff}.

3. Three-dimensional model of cement paste

A model that relates the three-dimensional microstructure of cement paste to impedance has already been described in Part I and elsewhere [10, 20, 21]. The electrical parameters assigned to each phase are given in Table I. The simulated impedance data from the model can be analysed in the same way as the experimental data was, and the value of k_{eff} determined. A plot of k_{eff} versus reaction time* for a simulated 0.4 w/c cement paste system is shown in Fig. 4, analogous to the plot in Fig. 1. Three of the five values displayed are at least a factor of two above 500, the highest value of k assigned to any phase (C–S–H) in the model. Therefore, an amplification mechanism must be present.

TABLE I Phase parameters used in three-dimensional impedance simulations

Phase	σ^a (S m^{-1})	k_r^b
Pore fluid	1.00	80
C–S–H	0.01	500
C_3S	3.60×10^{-8}	1
CH	3.60×10^{-8}	1

[a] σ is the d.c. conductivity.
[b] k_r is the relative dielectric constant.

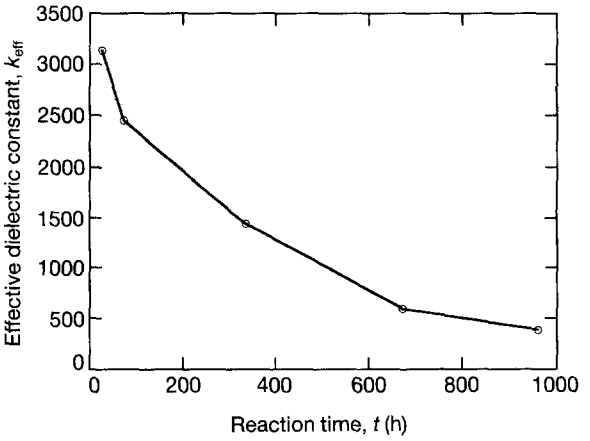

Figure 4 Three-dimensional model results for the change in the effective dielectric constant, k_{eff}, as a function of reaction time, t, for a 0.4 water:cement ratio model system. Reaction time is calculated from degree of reaction and published kinetic relationships [22].

It is crucial to note that the first three data points in Fig. 4, corresponding to the shortest reaction times, come from model systems in which the conductive pore phase is known directly from the model to be still percolated in the direction of the applied field [23]. Thus, isolation of the conductive phase (as in Fig. 3) is not required to produce amplification of the low frequency effective dielectric constant.

The model is not, however, capable of reproducing the full range of amplification that is observed experimentally, probably due to the limited resolution of its digital image-based format. The smallest unit of material that may be represented is 1 pixel, and therefore to achieve an amplification of $\times 100$ would roughly require a pore diameter of 100 pixels ($D = 100$, $d = 1$ in Equation 2). This degree of resolution is not currently possible.

In Fig. 5, a plot of k_{eff} versus water:cement ratio for model systems displays a trend similar to that observed in Fig. 2. All three data points in Fig. 5 are for models in which approximately the same fraction of cement initially present had been reacted, about 0.73,

* Reaction time is calculated from degree of reaction and published kinetic relationships [22].

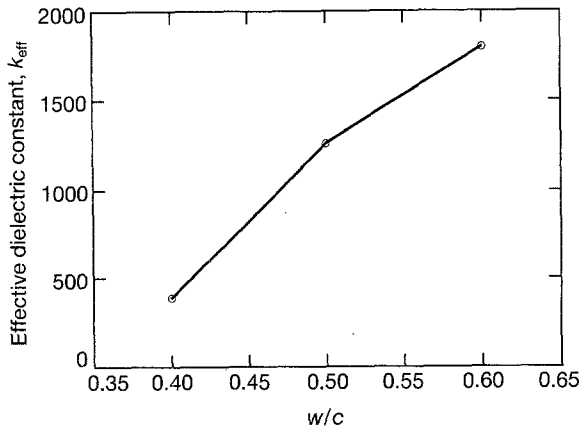

Figure 5 Three-dimensional model results for the effective dielectric constant, k_{eff}, of model systems with 0.73 of the cement hydrated.

but with different initial w/c values. Therefore, the volume fractions of pore fluid were different, increasing with increased w/c; whereas the volume fraction of C–S–H decreased with higher w/c. One might then expect the value of k_{eff} to be lower for higher w/c, because a smaller fraction of the high dielectric constant phase (C–S–H) was present. Since this is clearly not the case, again dielectric amplification by the microstructure must be taking place. The greater amplification corresponding to the higher water:cement ratios may be correlated with a higher value for D (Equation 2), rather than for d, since the latter is likely to be independent of water:cement ratio, especially for older pastes. In other words, d is related to the amount of product that has formed, while D is dependent on the amount of pore fluid (capillary porosity) that is present at any given time.

The three-dimensional computer models have thus shown that the high value of k_{eff} of the bulk arc of cement paste may be the result of microstructural amplification. The same trends were observed with respect to reaction time and water:cement ratio as seen experimentally. It was also shown that disconnection of the conductive phase (pore fluid) is not necessary to produce this amplification.

4. Two-dimensional models

The following two-dimensional models were developed to gain a better understanding of the kind of microstructural features that can give rise to a dielectric amplification mechanism, with and without a percolated highly conductive phase. Although two-dimensional, these models were formulated to capture the essential physics of three-dimensional microstructural features that can result in dielectric amplification. Both models are formed from 20×20 pixel digital images and consist of two phases, pore solution and C–S–H. The phases have the same properties as given in Table I, except that $\varepsilon_{C-S-H} = 1000$ instead of 500, for the sake of simplicity. The absolute value of the effective dielectric constant is not of great importance in these models, but, rather, the amount of amplification that may be produced based on the geometry of the microstructure.

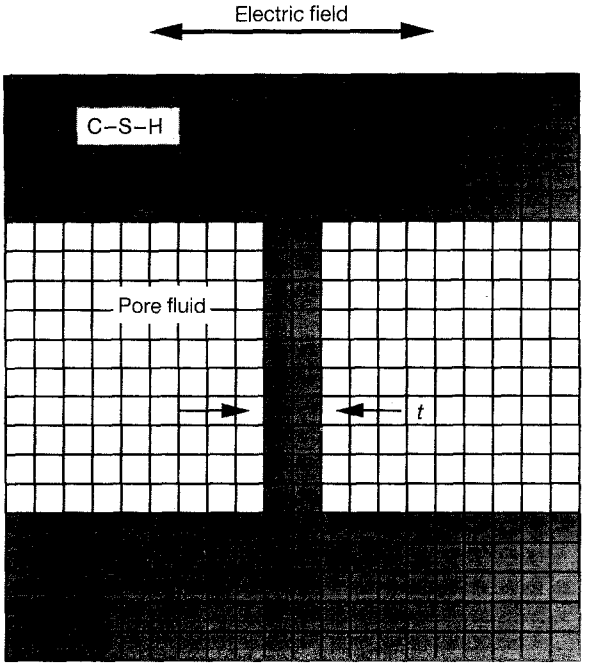

Figure 6 Schematic of the I model, shown with a crossbar thickness, t, of two pixels.

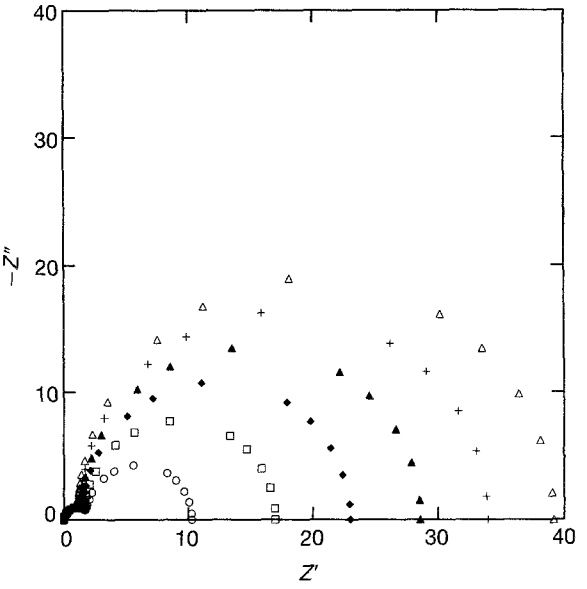

Figure 7 I model Nyquist plots at 0–900 GHz for different thickness, t, values. The peak frequency for each low frequency arc is 200 kHz: (○) $t = 1$, (□) $t = 2$, (◆) $t = 3$, (▲) $t = 4$, (+) $t = 5$ and (△) $t = 6$.

4.1. The I model

Fig. 6 shows a schematic of a model microstructure referred to here as the "I" model because the C–S–H phase forms a capital "I". The model represents an area between two reacting cement grains that are coated with C–S–H. Just enough product has formed to connect the two grains by a very thin layer of C–S–H. Continued reaction is simulated by thickening the connecting crossbar. The impedance is computed by applying a voltage in the direction shown on the figure. Fig. 7 shows the impedance curves for different thickness, t, values. Although it is overshadowed by the low frequency arc, a second, higher frequency arc does exist for each thickness, implying

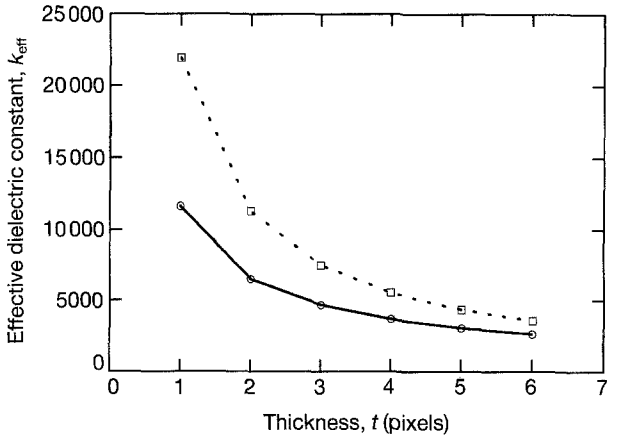

Figure 8 Effective dielectric constant, k_{eff}, as a function of crossbar thickness, t, for both the I (–○–) and T (–□–) models.

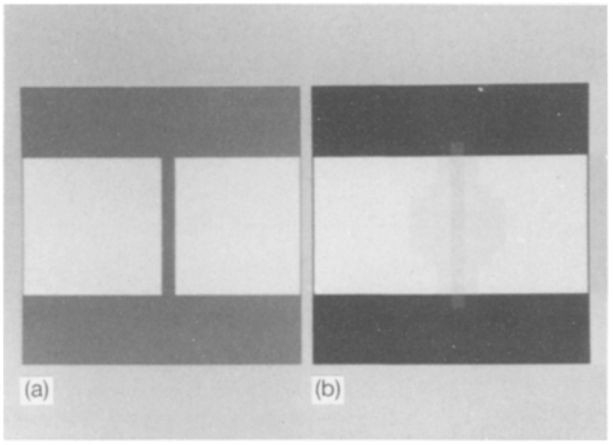

Figure 9 (a) I model with a crossbar thickness of 1 pixel, (b) corresponding current intensity plot, where white represents the highest value of current.

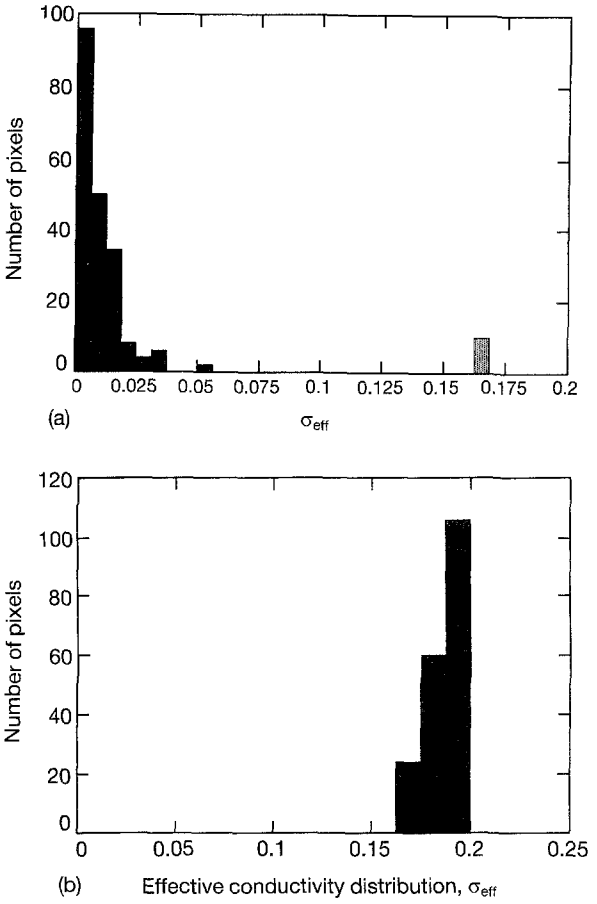

Figure 10 Effective conductivity distribution, σ_{eff}, functions for the I model (crossbar thickness of 1 pixel) for (a) C–S–H phase and (b) pore fluid phase with $\omega = 0$ (d.c.): (■) bulk C–S–H, (□) crossbar C–S–H.

that this microstructural arrangement has a series character [10]. Indeed the middle section of the I model is a series arrangement of C–S–H and pore fluid, although the upper and lower sections are arranged in parallel. As the thickness of the crossbar increases from 1–6 pixels, the composite resistance also increases as expected. The effective dielectric constant of the larger, lower frequency arc decreases with increasing t as shown in Fig. 8. As the thickness increases from 1–2 pixels, the amplification ratio, D/d, of the middle section is reduced from 20/1 to 20/2, and k_{eff} also drops by a factor of two. However, the value of k_{eff} of the composite when $t = 1$ is not $20 \times \varepsilon_{C-S-H} = 20000$, but closer to $10 \times \varepsilon_{C-S-H} = 10000$; since the middle section, from which comes the dielectric amplification, represents only 50% of the volume (area) of the composite. The value of k_{eff} in Fig. 8 roughly follows a $1/t$ power law for small t, as would be expected from the above analysis.

Analysing the current distribution in the model is useful to show the effect of microstructural geometry on the impedance properties. Fig. 9 shows a map of d.c. current intensity for the I model when $t = 1$. Fig. 9a represents the microstructure, where white is pore fluid and gray is C–S–H. Fig. 9b shows a gray scale image of the current intensity at each pixel where white equals high current and black equals low current, with various scales of gray for intermediate current values. It is apparent that some of the current is going around the crossbar and through some of the "bulk" C–S–H.

Fig. 10a, b shows the effective conductivity, σ_{eff}, distribution functions for each phase of the I model ($t = 1$). The effective conductivity for a given pixel is calculated by dividing the actual local current by the macroscopic field that has been applied to the total sample. The difference between the effective conductivity and the actual material conductivity for a given pixel is then a measure of the influence of the pixel's local environment on the current going through it. The effective conductivity distribution function is then just a histogram, showing what volume fraction of material has a given effective conductivity. More formally, the total average conductivity, σ_{comp}, of a multi-phase composite is defined by [12]

$$\sigma_{comp} = \frac{1}{\varepsilon_0}\frac{1}{V}\int_V d^3r\sigma(\vec{r})\varepsilon(\vec{r}) = \frac{1}{V}\int_V d^3r\sigma_{eff}(\vec{r}) \quad (3)$$

which can then be rewritten for a two-phase composite as

$$\sigma_{comp} = c_1\frac{1}{V_1}\int_{V_1} d^3r\sigma_{eff}(\vec{r}) + c_2\frac{1}{V_2}\int_{V_2} d^3r\sigma_{eff}(\vec{r}) \quad (4)$$

TABLE II Effective conductivity data for the I model

t	σ_{eff}^{a}		V_f^{b}		σ_{comp}^{c}	R^{d}
	C–S–H	Pore fluid	C–S–H	Pore fluid		
1	0.017 37	0.185 39	0.525	0.475	0.097	10.290
2	0.017 29	0.109 52	0.550	0.450	0.059	17.009
3	0.016 80	0.079 51	0.575	0.425	0.043	23.014
4	0.016 25	0.062 97	0.600	0.400	0.035	28.622
5	0.015 69	0.052 33	0.625	0.375	0.029	33.979
6	0.015 14	0.044 78	0.650	0.350	0.026	39.194

[a] σ_{eff} is the effective conductivity for a given phase, as defined in Equations 3–5.
[b] V_f is the volume fraction of a phase.
[c] σ_{comp} is the composite d.c. conductivity.
[d] $R = 1/\sigma_{comp}$ = the bulk resistance.

resulting in the equation

$$\sigma_{comp} = c_1\sigma_{eff}(1) + c_2\sigma_{eff}(2) \quad (5)$$

where $\sigma_{eff}(1)$ and $\sigma_{eff}(2)$ are the average value of the effective conductivity for phases one and two, respectively, $V_1 = c_1V$, $V_2 = c_2V$ are the partial volumes of each phase, $V_1 + V_2 = V$ is the total sample volume, and ε_0 is the original applied field. The values of the average effective conductivity for each phase are shown in Table II for each crossbar thickness. For each thickness in the I model, the effective conductivity of the C–S–H phase is increased above its assigned value of 0.01 (Fig. 10a), and the effective conductivity of the pore phase is decreased significantly from its assigned value of 1 (Fig. 10b). The composite resistance, R, is equal to $1/\sigma_{comp}$ for this square, two-dimensional geometry, and is also listed in Table II.

For the I model, it has been found that the frequency associated with the peak of the low frequency arc, ω_0, is the same for each thickness value. This implies that k_{eff} is a function of R via the following equation which defines k_{eff}

$$\omega_0 = \sigma/(k_{eff}\varepsilon_0) \quad (6)$$

where σ is the conductivity of the low frequency arc. As t increases, both σ and k_{eff} must decrease by the same factor in order to leave the value of ω_0 unchanged.

4.2. The T model

The T model microstructure shown in Fig. 11 is very similar to the I model, except that the lower section of the image has been changed from C–S–H to pore fluid. The crossbar in this case has extended from the cement grain into a pore, but not far enough to isolate one side of the pore from the other. This leaves the high conductivity pore phase continuous, as is the case in real three-dimensional cement paste. The impedance response for this system is shown in Fig. 12 for six different crossbar thicknesses. As with the I model, the composite resistance increases with increasing crossbar thickness; however, the magnitude of the resistance is much less. The size of the low frequency arc is also much smaller than in the I model, and the high frequency arc is much more visible. The value of k_{eff} associated with the low frequency arc follows the

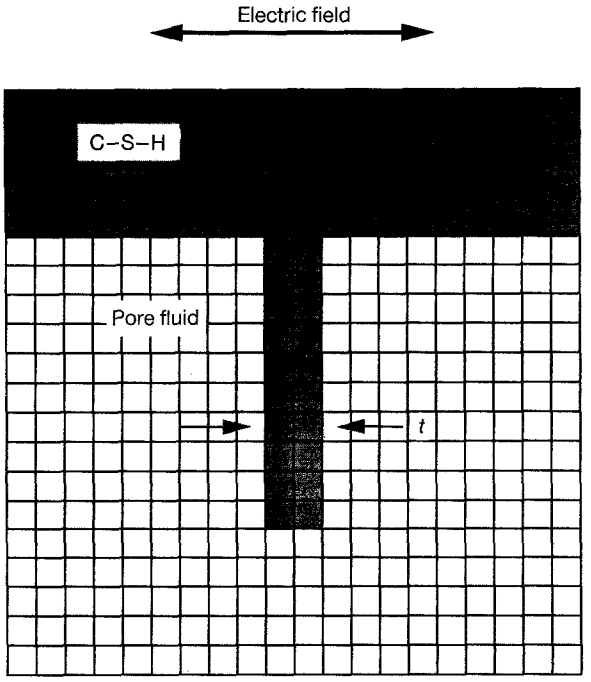

Figure 11 Schematic of T model, shown with a crossbar thickness, t, of 2 pixels.

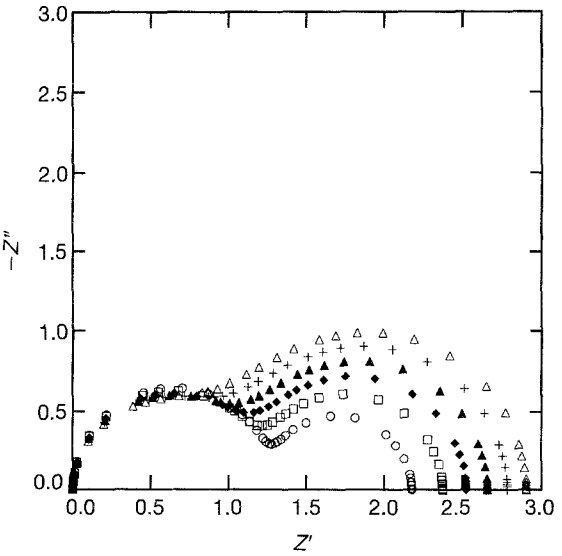

Figure 12 Nyquist plots for the T model at 0–900 GHz at different thickness values. The frequencies at the peaks of each low frequency arc are 1, 1.5, 2, 2.5 and 3 MHz for t = 1–6, respectively: (○) t = 1, (□) t = 2, (◆) t = 3, (▲) t = 4, (+) t = 5 and (△) t = 6.

TABLE III Effective conductivity data for the T model

t	σ^{a}_{eff}		V_f^{b}		σ^{c}_{comp}	R^{d}
	C–S–H	Pore fluid	C–S–H	Pore fluid		
1	0.019 84	0.626 68	0.275	0.725	0.460	2.175
2	0.019 48	0.593 77	0.300	0.700	0.421	2.373
3	0.018 76	0.578 40	0.325	0.675	0.397	2.522
4	0.018 00	0.569 33	0.350	0.650	0.376	2.657
5	0.017 25	0.564 79	0.375	0.625	0.359	2.782
6	0.016 53	0.563 00	0.400	0.600	0.344	2.903

[a] σ_{eff} is the effective conductivity for a given phase, as defined in Equations 3–5.
[b] V_f is the volume fraction of a phase.
[c] σ_{comp} is the composite d.c. conductivity.
[d] $R = 1/\sigma_{comp}$ = the bulk resistance.

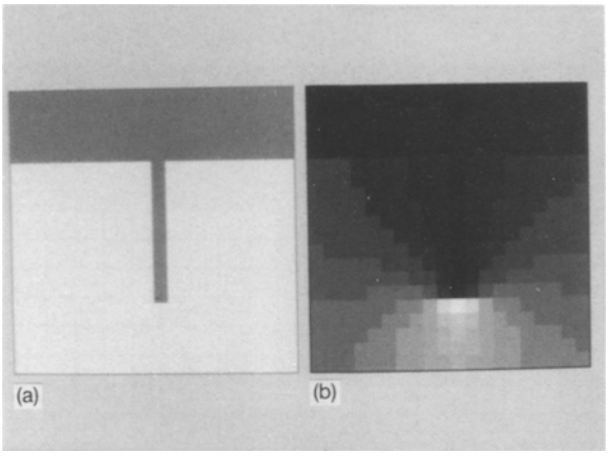

Figure 13 (a) T model with a crossbar thickness of 1 pixel, (b) corresponding current intensity plot, where white represents the highest value of current.

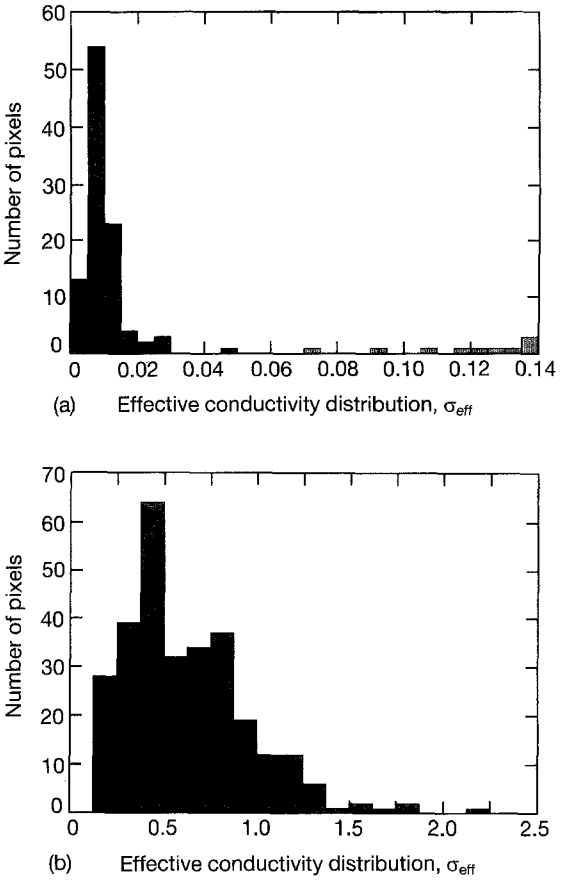

Figure 14 Effective conductivity distribution, σ_{eff}, functions in the T model (crossbar thickness of 1 pixel) for (a) C–S–H phase and (b) pore fluid phase, where $\omega = 0$ (d.c.): (■) bulk C–S–H, (□) crossbar C–S–H.

same trend as in the I model (see Fig. 8), but its value is higher, especially at smaller thickness values.

Fig. 13 shows a map of d.c. current intensity for the T model with a thickness, t, of 1 pixel. It is apparent that a significant amount of current simply flows around the crossbar through the much more conductive portion of the composite, thus significantly reducing the composite resistance, and, therefore, the size of the low frequency arc. Distribution functions of effective conductivities for the T model ($\omega = 0$) with a crossbar thickness of 1 pixel are shown in Fig. 14 for C–S–H (a) and pore fluid (b). Table III lists the average single phase effective conductivities for the T model at different thicknesses, analogous to Table II. It is evident from Fig. 14b and Fig. 13 that the pore fluid in the T model has a much wider distribution of effective conductivities than the pore fluid in the I model. The distribution of effective conductivities for C–S–H in the T model is not much different than in the I model.

The flow of current around the crossbar in Fig. 13 is not too surprising, and raises the question of why, since the crossbar is providing the mechanism for dielectric amplification, should the T model have a higher value of k_{eff} than the I model?

The answer to this question lies in the effective conductivities of the crossbar pixels for each model. The following explanation, applicable to any crossbar thickness, compares the effective conductivities of the crossbar pixels for both the I and the T models, for a thickness of 1 pixel. Consider the crossbar pixels to be numbered 1–10, starting with the first pixel of the crossbar nearest the top, as pictured in Figs 6 and 11.

Fig. 15 shows a plot of effective conductivity versus the position of the crossbar pixel for both the I and T models when the applied frequency is zero (d.c.). As expected, the effective conductivity of crossbar pixels in the I model is higher, and relatively constant along the bar. The crossbar pixels of the T model, on the other hand, have overall lower effective conductivities, and the pixels toward the end of the crossbar have

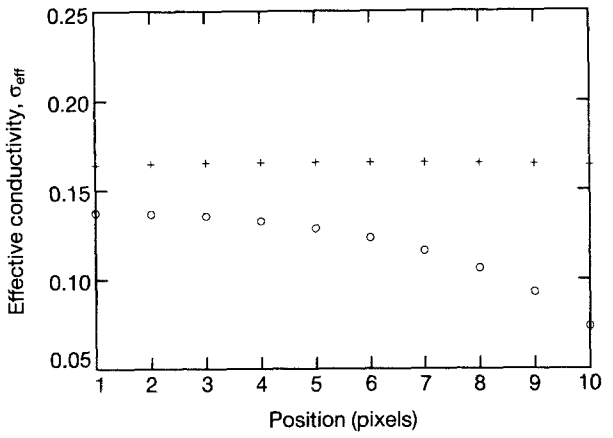

Figure 15 Effective conductivity as a function of pixel position along the crossbar at zero frequency (d.c.) with a crossbar thickness of 1 pixel, for both the I (+) and T (○) models.

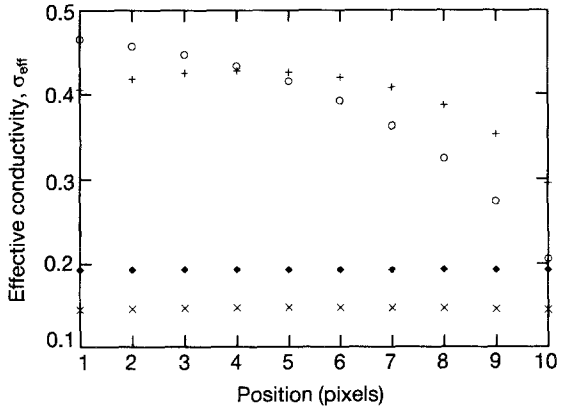

Figure 16 Effective conductivity as a function of pixel position along the crossbar at the peak frequency (I, 200 kHz; T, 1 MHz) with a crossbar thickness of 1 pixel: (○) real T, (+) imaginary T, (◆) real I and (×) imaginary I.

significantly lower effective conductivities than those near the top. Near the top of the crossbar it is easier for the current to go through the crossbar than travel all the way to the bottom to go around the crossbar, which will tend to increase the effective conductivity near the top. Near the bottom of the crossbar, however, current may easily travel around the tip through the more conductive pore fluid, thus reducing the effective conductivity of the pixels near the bottom of the crossbar.

The situation is quite different for the two models at the peak frequency ω_0. Fig. 16 shows the effective conductivity (both real and imaginary) for the crossbar pixels at the peak of the low frequency arc for each model. In this case, the effective conductivities of the crossbar pixels in the T model are higher than those of the I model for both real and imaginary components. The geometry of the T model is such that the microstructural feature responsible for dielectric amplification (crossbar) has a higher effective conductivity at the peak frequency than its counterpart in the I model. In other words, more current passes through the crossbar in the T model, producing greater dielectric amplification. It is important to recall that the T model has a well percolated high d.c. conductivity phase. In fact, at least for the I and T models, a percolated high d.c. conductivity phase actually seems to produce *higher* values of k_{eff}.

5. Conclusions

The dielectric response of hydrating cement paste is dependent on the developing microstructure and the arrangement of microstructural phases. Impedance simulations from digital image-based models have successfully reproduced the main features of the dielectric response of cement paste, and provide valuable insight into the relationship between microstructure and measured impedance. The current distributions and effective conductivities obtained through the digital image technique are excellent examples of how the data obtainable from computer modelling can be used in understanding observed phenomena.

The extremely high effective dielectric constants determined from the bulk arcs of cement paste may be explained by an amplification mechanism produced by microstructural arrangements in hydrating cement paste. Amplification could result from relatively large capillary pores, D, and thin product layers, d, that block or redirect current flow in the impedance experiment. It is thus possible to produce dielectric amplification without disconnecting, or depercolating, the conductive, capillary pore phase. In fact, *higher* effective dielectric constants may be obtained from microstructures in which the conductive phase remains connected. This is consistent with what is known about the continued presence of continuous capillary pores in cement pastes that have achieved high degrees of hydration [23].

Moderate amplification of the effective dielectric constant is found in the three-dimensional, digital image-based model of cement paste, probably due to the finite resolution (1 pixel = 1 μm) of the pixel-based model. Higher values of k_{eff} would be obtained if the resolution were to be increased. The I and T models suggest that the capillary pore structure is highly tortuous, and, at early reaction times, thin product layers extend into capillary pores and connect reacting cement grains.

The drop in k_{eff} with degree of hydration can be explained by the changing microstructural features that control dielectric amplification. If D is taken as a measure of the size of the pore fluid-filled capillary pores, and d is taken as a measure of the size of the reaction product thicknesses separating or extending into these pores, then as the reaction products grow, capillary pore sizes are reduced (D decreases), and reaction products extending into the pore space thicken (d increases). Both of these effects serve to decrease amplification. The increase in effective dielectric constant with water:cement ratio, at equal degrees of hydration, is a result of larger capillary pores being present in the microstructure at the higher water:cement ratios, but with nearly the same value of product thickness, d. Thus the amplification ratio, D/d, will be increased as water:cement ratio increases at roughly equal degrees of hydration.

Acknowledgements

The authors would like to acknowledge the National Science Foundation's Center for Science and Technology for Advanced Cement Based Materials, under grant number DMR-08432, for financial support. Supercomputing facilities were provided by the National Center for Super Computing Applications at the University of Illinois at Champaign-Urbana, under grant number DMR-920024N.

References

1. C. A. SCUDERI, T. O. MASON and H. M. JENNINGS, *J. Mater. Sci. Lett.* **7** (1988) 1056.
2. B. J. CHRISTENSEN, T. O. MASON and H. M. JENNINGS, *J. Amer. Ceram. Soc.* **75** (1992) 939.
3. P. GU, Z. XU, P. XIE and J. J. BEAUDOIN, *Cem. Conc. Res.* **23** (1993) 531.
4. Z. XU, P. GU, P. XIE and J. J. BEAUDOIN, *ibid.* (in press).
5. *Idem, ibid.* (in press).
6. P. GU, P. XIE and J. J. BEAUDOIN, *ibid.* **23** (1993) 581.
7. P. GU, P. XIE, J. J. BEAUDOIN and R. BROUSEAU, *ibid.* **22** (1992) 833.
8. *Idem, ibid.* **23** (1993) 157.
9. P. XIE, P. GU, Z. XU and J. J. BEAUDOIN, *ibid.* **23** (1993) 359.
10. R. T. COVERDALE, B. J. CHRISTENSEN, T. O. MASON, H. M. JENNINGS, D. P. BENTZ and E. J. GARBOCZI, *J. Amer. Ceram. Soc.* (to be submitted).
11. "Impedance Spectroscopy: Emphasizing Solid Materials and Systems", edited by J. R. MacDonald (Wiley, New York 1987) p. 39.
12. Z. HASHIN, *J. Appl. Mech.* **50** (1983) 481.
13. J. R. HASTED, "Aqueous Dielectrics" (Chapman & Hall, London, 1973) p. 137.
14. R. T. COVERDALE, E. J. GARBOCZI, B. J. CHRISTENSEN, T. O. MASON and H. M. JENNINGS, *J. Amer. Ceram. Soc.* **76** (1993) 1153.
15. W. J. McCARTER, S. GARVIN and N. BOUZID, *J. Mater. Sci. Lett.* **7** (1988) 1056.
16. D. M. GRANNAN, J. C. GARLAND and D. B. TANNER, *Phys. Rev. Lett.* **46** (1981) 375.
17. D. J. BERGMAN and Y. IMRY, *ibid.* **39** (1977) 1222.
18. D. STROUD and D. J. BERGMAN, *Phys. Rev. B* **25** (1982) 2061.
19. R. P. FEYNMAN, R. B. LEIGHTON and M. SANDS, "The Feynman Lectures on Physics", Vol. 2 (Addison-Wesley, Reading, MA, 1964) p. 10–2.
20. R. T. COVERDALE, E. J. GARBOCZI and H. M. JENNINGS, *J. Comp. Mater. Sci.* (submitted).
21. R. T. COVERDALE, PhD thesis, Northwestern University, IL (1993).
22. H. F. W. TAYLOR, "Cement Chem." (Academic Press, San Diego, CA, 1990) p. 159.
23. D. P. BENTZ and E. J. GARBOCZI, *Cem. Concr. Res.* **21** (1991) 325.

Received 18 January
and accepted 21 March 1994